

Article

An Experimental Evaluation of the Feasibility of Inferring Concentrations of a Visible Tracer Dye from Remotely Sensed Data in Turbid Rivers

Carl J. Legleiter ^{1,*}, Paul V. Manley II ², Susannah O. Erwin ³ and Edward A. Bulliner ³¹ U.S. Geological Survey, Integrated Modeling and Prediction Division, Golden, CO 80403, USA² Missouri University of Science and Technology, Rolla, MO 65409, USA; pvm88b@mst.edu³ U.S. Geological Survey, Columbia Environmental Research Center, Columbia, MO 65201-8709, USA; serwin@usgs.gov (S.O.E.); ebulliner@usgs.gov (E.A.B.)

* Correspondence: cjl@usgs.gov; Tel.: +1-303-271-3651

Received: 17 October 2019; Accepted: 20 December 2019; Published: 22 December 2019



Abstract: The movement of contaminants and biota within river channels is influenced by the flow field via various processes of dispersion. Understanding and modeling of these processes thus can facilitate applications ranging from the prediction of travel times for spills of toxic materials to the simulation of larval drift for endangered species of fish. A common means of examining dispersion in rivers involves conducting tracer experiments with a visible tracer dye. Whereas conventional in situ instruments can only measure variations in dye concentration over time at specific, fixed locations, remote sensing could provide more detailed, spatially-distributed information for characterizing dispersion patterns and validating two-dimensional numerical models. Although previous studies have demonstrated the potential to infer dye concentrations from remotely sensed data in clear-flowing streams, whether this approach can be applied to more turbid rivers remains an open question. To evaluate the feasibility of mapping spatial patterns of dispersion in streams with greater turbidity, we conducted an experiment that involved manipulating dye concentration and turbidity within a pair of tanks while acquiring field spectra and hyperspectral and RGB (red, green, blue) images from a small Unoccupied Aircraft System (sUAS). Applying an optimal band ratio analysis (OBRA) algorithm to these data sets indicated strong relationships between spatially averaged reflectance (i.e., water color) and Rhodamine WT dye concentration across four different turbidity levels from 40–60 NTU. Moreover, we obtained high correlations between spectrally based quantities (i.e., band ratios) and dye concentration for the original, essentially continuous field spectra; field spectra resampled to the bands of a five-band imaging system and an RGB camera; and both hyperspectral and RGB images acquired from an sUAS during the experiment. The results of this study thus confirmed the potential to map dispersion patterns of tracer dye via remote sensing and suggested that this empirical approach can be extended to more turbid rivers than those examined previously.

Keywords: tracer; dye; concentration; river; turbidity; Rhodamine; hyperspectral; multispectral; UAS; dispersion

1. Introduction

Flow patterns in rivers affect the movement of constituents suspended or dissolved within the water column or drifting at the water surface, including pollutants, nutrients, and organisms. The mechanisms by which these materials are redistributed by the flow are collectively referred to as dispersion processes. An understanding of these processes can inform a broad range of applications

and numerical models of dispersion have been used to simulate the spread of hazardous substances within river channels. For example, dispersion modeling can help guide emergency management by predicting how spills of oil and other toxic materials move through river systems, estimating residence times, and identifying areas where contaminants might accumulate. This type of information can help agencies issue timely warnings and direct remediation efforts appropriately [1,2]. In a biological context, detecting the presence and movement of harmful algal blooms can help to understand their impact on aquatic ecosystems and human health [3]. Erwin et al. [4] used a dispersion model to characterize the drift of endangered pallid sturgeon larvae on the Missouri River.

An intuitive and effective way to gain insight regarding dispersion processes is by conducting tracer experiments that involve adding a substance to the flow and measuring changes in its concentration as the material spreads through the channel. Many tracer studies are performed using a visible dye such as Rhodamine WT, which can be considered a conservative tracer for most surface water applications (but not in cases where hyporheic exchange and/or groundwater flow are of interest due to sorption of Rhodamine WT to sediment [5]). Dye concentrations can be measured in situ by submersible fluorometers (also known as sondes), but typically, these sensors are only deployed at a small number of fixed locations to record variations in concentration over time. This approach yields information at specific points that can be used to evaluate predictions from one-dimensional (1D) dispersion models that predict how constituent concentrations vary along a channel and over time. Although 1D models are useful for contaminant-oriented applications such as estimating travel times, the output from these models is averaged across the channel width and thus fails to provide information on lateral concentration gradients, eddies, and other small-scale flow patterns. This level of detail often is of greater interest in biological studies and two-dimensional (2D) dispersion models and particle tracking algorithms have been developed to provide greater spatial resolution both along and across the channel. Moreover, whereas conventional in situ instrumentation (i.e., sondes) might be sufficient for validating 1D models, this approach fails to characterize the complex spatial patterns of dispersion that emerge even when a single pulse of dye is released instantaneously. Remote sensing, in contrast, could facilitate dispersion studies by providing the kind of spatially distributed observations of dye concentration needed to validate 2D numerical models and support applications seeking to resolve subtle, small-scale features of the flow field.

The potential to map dispersion patterns via remote sensing was first demonstrated in coastal environments [6,7]. Clark et al. [6] showed that passive optical image data could be used to estimate Rhodamine WT dye concentrations in the surf zone and identify eddies and other small-scale structures (on the order of 10 m) associated with the dispersion of a dye pulse. More importantly, this study established the physical basis for inferring dye concentrations from observations of water color: adding Rhodamine WT to a water body decreases the upwelling spectral radiance in the green portion of the visible spectrum from 530–570 nm due to absorption by the dye, whereas reflectance by the dye increases the upwelling spectral radiance in red and near-infrared (NIR) wavelengths from 570–750 nm. Clark et al. [6] found that the greatest changes in radiance occurred at 553 nm, an absorption feature associated with the dye, and 595 nm, where dye reflectance peaks. This absorption feature occurred at a shorter wavelength than the fluorescent excitation band of pure Rhodamine WT (557 nm), whereas the peak occurred at a longer wavelength than the dye's inherent emission band (582 nm) [8]. These differences were attributed to overlap between the absorption and reflectance spectra of Rhodamine WT near 570 nm. Irrespective of the specific wavelengths involved, Clark et al. [6] hypothesized that the ratio of the upwelling spectral radiance measured in an absorption band to that measured at a reflectance peak would be proportional to dye concentration. Support for this hypothesis was provided by a pair of near-shore tracer experiments in which band ratio values calculated using data from both a two-band (530–560 nm and 590–620 nm) camera and a hyperspectral imaging system were strongly correlated with in situ concentration measurements. The empirical, linear relations reported by Clark et al. [6] were strongest at low concentrations (<20 ppb) but became increasingly non-linear at higher concentrations, with the nature (convexity or concavity) and degree of non-linearity

varying as a function of the inherent optical properties (i.e., absorption and back-scattering coefficients) of the water itself. These results suggest that reliable inference of dye concentrations from remotely sensed data might be contingent upon the background optical characteristics of the water body. Powers et al. [9] also showed that image data acquired from a small unoccupied aircraft system (sUAS) could be used to map another type of visible dye, called fluorescein, following its injection into a small reservoir.

More recently, the potential for remote sensing of tracer dye concentrations in river systems also has been established [10,11]. Using data acquired from a unique experimental facility with a sinuous outdoor flume, Baek et al. [11] tested the feasibility of estimating dye concentrations from RGB (red, green, blue) images acquired from a sUAS. Accurate concentration maps were produced from the relatively basic, three-band image data by training an artificial neural network to account for spatial variations in water depth and bottom composition that modified the relationship between image brightness and dye concentration on a local basis. Legleiter et al. [10] developed a more spectrally based approach using hyperspectral images acquired from a sUAS deployed above the same experimental channel as in [11] and field spectra and multi- and hyperspectral image data from the Kootenai River, a large natural river in northern Idaho, USA. An optimal band ratio analysis (OBRA) algorithm [12,13] was modified to identify wavelength combinations that yielded strong correlations between a spectrally based quantity X and dye concentration C . Relative to the machine learning technique employed by Baek et al. [11], the OBRA framework provided greater insight as to how reflectance varies with concentration and a more flexible, readily interpretable means of identifying specific wavelength combinations that yield strong relationships between dye concentrations and spectrally based quantities. Legleiter et al. [10] reported very strong (R^2 from 0.94 to 0.99) relationships between X and C across a broad range of visible wavelengths for all of the data sets considered: sUAS-based hyperspectral images from the outdoor flume, field spectra collected from a boat on the Kootenai River, and hyperspectral images and high-resolution aerial photographs acquired from a manned aircraft along the Kootenai. In addition, Legleiter et al. [10] showed that X vs. C relations derived from field spectra could be applied to hyperspectral images and that concentrations could be estimated nearly as reliably from RGB images as from hyperspectral data.

These previous studies imply that remote sensing could become a powerful tool for mapping tracer patterns in rivers and thus help to advance our understanding of dispersion processes. However, because prior research was conducted in clear-flowing streams, a key question remains: can this approach also be applied in more turbid settings? Whereas the Kootenai is an exceptionally clear river [14] and the outdoor flume used by Baek et al. [11] and Legleiter et al. [10] was both clear and shallow, many rivers of interest are large, deep, and, perhaps most importantly, far more turbid. The presence of greater turbidity could pose a challenge to remote sensing of tracer dye concentrations because this approach is based on spectrally exploiting the change in water color caused by the presence of the dye. If the water is laden with sediment and has a pronounced background color, the reflectance signal associated with the dye might be obscured. For example, the contrast between clear water with varying levels of Rhodamine WT dye and turbid water with no dye is illustrated in Figure 1, which compares field spectra from a previous tracer study on the clear-flowing Kootenai River [10] to turbid but dye-free spectra acquired during the experiment described herein. This comparison suggests that although elevated turbidity increases the overall brightness of the water across the visible and NIR portion of the spectrum, the presence of dye with distinctive reflectance and absorption features at certain key wavelengths might enable concentrations to be inferred even in turbid water. In any case, although the results reported by Baek et al. [11] and Legleiter et al. [10] are encouraging, further work is needed to test the feasibility of estimating tracer concentrations from remotely sensed data across a broader range of river conditions, particularly higher levels of turbidity. In addition, given the sensitivity of band ratio-based reflectance–concentration relationships to background water characteristics observed by Clark et al. [6], another open question is what kind of remotely sensed data might be suitable for retrieving dye concentrations in more turbid waters.

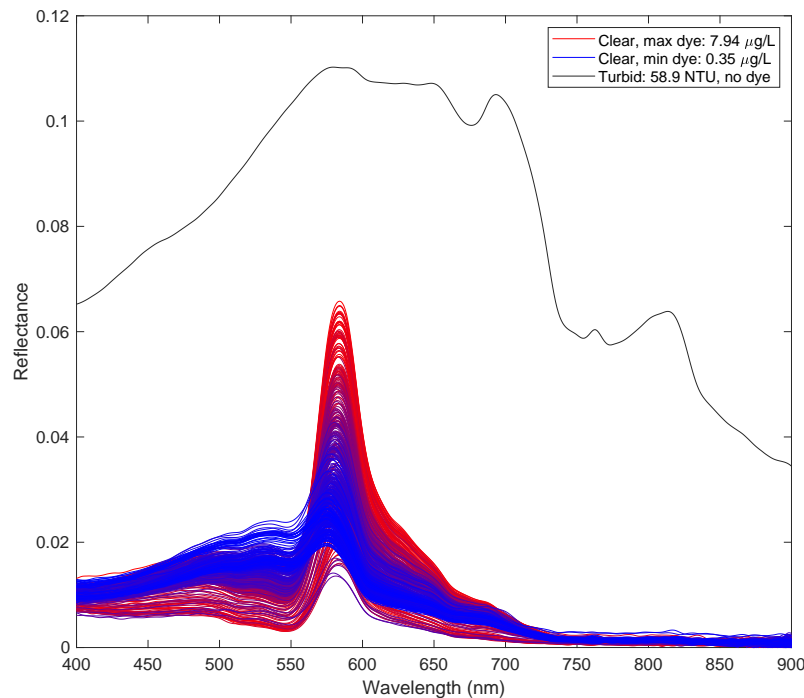


Figure 1. Contrast between field spectra collected from highly turbid water with no dye during the experiment described herein and field spectra from a clear-flowing river in a previous study [10]. The red and blue lines represent field spectra recorded along with dye concentrations during multiple transects across the Kootenai River during the passage of a plume of Rhodamine WT dye. The line color for each individual spectrum is based on the corresponding dye concentration measured in situ, ranging from blue for low, near-background values to a maximum observed concentration of nearly 8 $\mu\text{g/L}$. The turbidity of the Kootenai River when these spectra were collected was approximately 2 NTU.

As a precursor to tracer studies planned for the Missouri River, which is a much more turbid fluvial environment than those we have examined to date, we conducted an experiment to assess the potential to remotely sense dye concentrations in water bodies with greater turbidity. The planned tracer studies are intended to support ongoing investigations of endangered pallid sturgeon (*Scaphirhynchus albus*), specifically the dispersion of larvae within the Missouri River and its tributaries [4]. Because dispersal (a biological term that encompasses both physical dispersion by the flow and the active, behavioral processes of organisms) of early-life-stage sturgeon is a critical phase of the species' life history that could represent a potential recruitment bottleneck [15], tracer studies could help ecologists better understand and model the dispersal process. More broadly, the work presented herein is germane to a number of other applications outside the immediate context of sturgeon. For example, the ability to map spatial patterns of tracer concentration in not only clear-flowing but also more turbid rivers would facilitate the development and testing of numerical dispersion models used to predict the spread of contaminants and estimate residence times [1,2].

Although our long-term objective is to obtain spatially distributed information on tracer dye concentrations to facilitate validation of 2D numerical models of the dispersion process, the purpose of this proof-of-concept investigation was to assess the feasibility of applying this approach in turbid river channels. To achieve this goal, we performed an experiment using tanks in which we could manipulate tracer dye concentration and turbidity levels and focused on spatially averaged spectral responses rather than spatial reflectance patterns within the small tanks. More specifically, this paper presents results from an experiment designed to address the following questions:

1. Can reliable estimates of dye concentration be inferred from remotely sensed data across a range of turbidity levels higher than those observed in previous tracer studies in clear-flowing streams?
2. Are continuous field spectra required to measure dye concentrations in turbid waters, or would broader-band sensors be sufficient for this purpose?
3. Can dye concentrations be mapped from hyperspectral and RGB images acquired from sUAS?

2. Materials and Methods

The experiment was conducted at the United States Geological Survey (USGS) Columbia Environmental Research Center (CERC) in Columbia, Missouri, USA, on 2 April 2019, and involved manipulating dye concentration and turbidity while acquiring field spectra and sUAS-based hyperspectral and RGB images. This approach allowed us to examine how the nature and strength of relationships between reflectance and concentration varied for different levels of turbidity. All data collected during this study are included in a data release available through the USGS ScienceBase repository [16].

2.1. Manipulation and in situ Measurement of Turbidity and Dye Concentration

Water sourced from a deep well and stored in a pond at CERC was pumped into two circular, 1.83-m diameter tanks and filled to a depth of approximately 0.5 m. The interiors of the tanks were painted black to minimize reflectance from their sidewalls or bottoms. At the beginning of each experimental run, Rhodamine WT was added to the tanks and rapidly became well-mixed with minimal stirring. The amount of dye injected was calculated based on the known volume of water in the tank and each of six target concentrations: 0, 2, 6, 9, 12, and 20 ppb.

Fine-grained sediment derived locally from the floodplain of the Missouri River was purchased from a commercial vendor near Jefferson City, Missouri. A sample of this material was sent to the USGS Central Midwest Water Science Center to quantify the grain size distribution following standard USGS methods. This analysis indicated that the sediment was a sandy loam with 67.9% sand, 24.5% silt, and 7.6% clay, with a median particle size of approximately 0.15 mm. Sediment was added to each tank and agitated with pumps to place the material into suspension. The turbidity of the water in the tanks then decreased gradually over time as the sediment settled.

An in situ sensor, a Turner C3 submersible fluorometer, was placed within each tank and used to record time series of turbidity and dye concentration with a 15-s logging interval. All of the instruments involved in this study used a common time standard (Global Positioning System (GPS) time) to enable synchronization of the various data sources. The sondes measured dye concentration as a function of fluorescence and were calibrated using a two-point (0 and 10 ppb) procedure established by the manufacturer. To create calibration solutions for fluorescence, the same pond water pumped into the tanks for the experiment was used to dilute a manufacturer-recommended standard. We executed this calibration protocol immediately prior to the experiment so that the water used to calibrate the sondes would be representative of that used during data collection. Each sonde also included a turbidity sensor, which we calibrated using a similar two-point procedure. The sondes were calibrated at 0 (deionized water) and 100 NTU using a calibration standard diluted with deionized water. The calibration for each sensor in each sonde was tested and found to read within 5% for both low (1 ppb) and high (30 ppb) test dilutions of dye and both low (10 NTU) and high (400 NTU) test dilutions of the turbidity standard.

By the time spectral measurements and image acquisition commenced at 13:19 (UTC) on 2 April 2019, the turbidity had reached a mean of 58.9 NTU and continued to decrease until the last round of measurements was made at 21:22, when the mean turbidity was 43.1 NTU. The field spectra and image data sets described below were subdivided on the basis of turbidity into four distinct ranges: 40–45, 45–50, 50–55, and 55–60 NTU (Table 1). For context, at the nearest USGS gauge on the Missouri River with long-term turbidity data (Hermann, #06934500), median daily-average turbidity values varied by month and ranged from a low of 14.7 NTU in January to a high of 207 NTU in June.

Table 1. Summary of data sets acquired during the experiment, organized into four distinct turbidity ranges. Hyperspectral images were selected to coincide as closely as possible with the timing of the field spectra and RGB images were selected to match the timing of the hyperspectral images.

Turbidity Range (NTU)	Nominal Dye Concentration (ppb)	Field Spectra Sets	Field Spectra Time Range (UTC)	Hyperspectral Image Times (UTC)	RGB Image Times (UTC)
40–45	2	4,5,6	16:20 - 17:20	16:23, 17:03	16:22, 16:51
	9	6,7	20:14–20:48	20:28, 20:39	20:28, 20:39
	20	6,7	20:25–21:22	20:28, 20:39	20:28, 20:39
45–50	2	3	15:49–16:00	15:55, 15:59	15:55, 16:02
	12	5,6,7	16:57–17:59	16:58, 17:36	16:51, 17:36
	9	3,4,5	18:59–20:00	19:01, 19:47	19:01, 19:59
50–55	20	3,4,5	19:11–20:12	19:11, 20:08	19:11, 20:08
	2	2	15:24–15:35	15:26	15:26
	12	2,3,4	15:37–16:43	15:55, 16:41	16:02, 16:41
	9	2	18:36–18:47	18:36, 18:43	18:36, 18:43
55–60	20	2	18:48–18:58	18:49, 18:57	18:49, 18:55
	6	13	13:19–13:32		
	0	13	13:37–13:48		
	2	1	14:59–15:10		
	12	1	15:11–15:22	15:17, 15:20	15:21, 15:21
	9	1	18:09–18:20		
	20	1	18:21–18:32		

2.2. Field Spectra

Ground-based measurements of spectral reflectance (i.e., field spectra) were used to quantify the relationship between reflectance and dye concentration for each of the four turbidity ranges. To collect these data, we placed an Analytical Spectral Devices HandHeld2 Pro spectroradiometer [17] with a 5° fore-optic, hereafter referred to as the ASD, on a tripod located between the two tanks, each of which had a distinct dye concentration. This arrangement allowed us to efficiently sample two different concentrations by pivoting the ASD to first view one tank and then the other, without having to move the ASD or the laptop computer used to control the instrument and store the spectra. Pivoting the instrument implied that the two tanks were viewed from opposite directions, but on the basis of our visual observations of the water in the tanks, we assumed that the volume reflectance of the water was not strongly anisotropic and thus insensitive to differences in viewing orientation. The ASD was operated in reflectance mode based on a white reference established by measuring a Labsphere Spectralon [18] calibrated diffuse reflectance standard. Dividing the digital counts for each target spectrum by the digital counts for the white reference panel yielded relative reflectance spectra in units of percent. In addition, a dark current correction was performed by closing the shutter on the ASD prior to each white reference measurement.

A given measurement sequence, which we refer to as a field spectra set, involved collecting reflectance data from one of the tanks and proceeded as follows:

1. Calibrate the instrument by pointing the ASD at the Spectralon panel to establish the white reference and dark current correction.
2. Record five spectra from the Spectralon panel to document the illumination conditions (i.e., solar position and cloud cover) at the beginning of the field spectra set.
3. Use a swivel on the tripod to pivot the ASD toward the tank and orient the fore-optic so as to only view the water toward the middle of the tank, avoiding any shadows cast by the sides of the tank. A typical viewing angle was approximately 15° off-nadir.
4. Initiate a measurement sequence consisting of 40 individual field spectra, saved once every 15 s over a 10-min time period. This protocol provided a large sample size to capture variability

related to changes in illumination, reflectance from the water surface (i.e., sun glint), and the passage of foam or any other objects floating within the tank.

5. Pivot the ASD back toward the Spectralon panel and record an additional five panel spectra to characterize any changes in illumination that occurred during the field spectra set.

The file save time for each field spectrum was used to link the reflectance data to the in situ measurements of dye concentration and turbidity made by the sonde at that time. Mean values of concentration and turbidity over the 10-minute duration of a field spectra set were assigned to each of the spectra within that set. The resulting paired observations of reflectance and concentration were used to examine relationships between the color of the water and the amount of dye present within the two tanks for each of the four turbidity ranges observed during the experiment.

2.3. Remotely Sensed Data

Hyperspectral image data were collected with a Headwall Nano-Hyperspec [19], hereafter referred to as the Nano. This pushbroom sensor measures upwelling spectral radiance in visible and NIR wavelengths from 400–1000 nm. In this study, the Nano was deployed from a DJI Matrice 600 Pro [20] sUAS by mounting the sensor on a DJI Ronin-MX gimbal [21] attached to the Matrice. Prior to each flight, the Nano was calibrated by collecting a dark reference with the lens cap on and establishing a white reference by pointing the instrument toward a 25.4 × 25.4 cm Labsphere Spectralon [18] calibrated diffuse reflectance standard that reflected 99% of the incident radiation.

The sUAS executed a flight plan that involved making multiple passes back and forth above the tanks at a constant height of 30 m above ground level. Because the Nano is a pushbroom, line-scanning instrument, producing a two-dimensional spatial image required the sUAS to be in motion, rather than hovering in a single fixed location. Stabilization of the sensor payload by the gimbal facilitated post-processing of the hyperspectral image data. The raw images were radiometrically corrected (i.e., converted from digital numbers to radiance) in the Headwall SpectralView software package. This program also was used to orthorectify the images based on latitude and longitude information and measurements of sensor orientation recorded by a GPS receiver and inertial measurement unit (IMU) aboard the aircraft during each flight. This process yielded images with a ground sampling distance of 2 cm.

Calibration tarps were placed on the ground adjacent to the tanks to ensure that the Nano images included a clearly visible reference object with a known reflectance. The tarps were used as a white reference within the ENVI version 5.5.2 software package [22] to convert the radiance data to relative reflectance units comparable to the field spectra. Time stamps for the Nano data were used to select for further analysis only the two images acquired closest in time to when the field spectra sets for a given dye concentration and turbidity range were recorded (Table 1). This approach ensured that both the ground- and sUAS-based observations of spectral reflectance captured the same water characteristics under similar illumination conditions.

Conventional visible images also were obtained during the experiment. These data were collected from a DJI Mavic Pro sUAS equipped with a built-in 12 megapixel camera [23]. RGB images were acquired on a 2-s interval while the sUAS hovered in a fixed position at a constant height of approximately 30 m above the tanks. Timestamps were used to identify the RGB images closest in time to when the Nano images were acquired to maximize consistency among the two types of remotely sensed data and the field spectra. No further pre-processing of the RGB data was performed prior to the analysis described below.

The hyperspectral and RGB image data sets listed in Table 1 were related to the corresponding in situ measurements of dye concentration and turbidity made in each tank during the flights. For both types of remotely sensed data, polygons were digitized to delineate the water in the center of each tank in each image (Figure 2a,b). The pixel values from within these polygons were extracted from the images and spatially averaged to obtain reflectance spectra for the Nano images (Figure 2c) and digital numbers in three bands for the RGB images (Figure 2d).

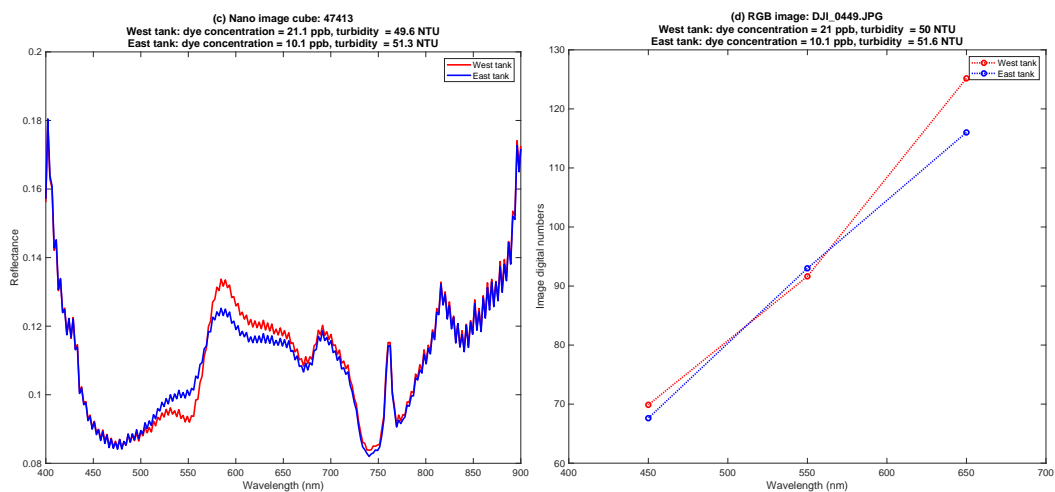
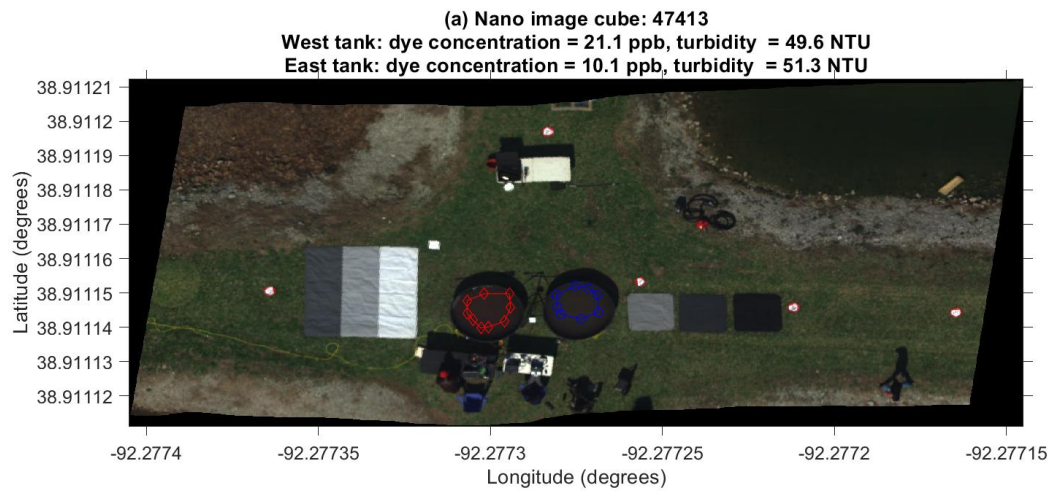


Figure 2. (a) Example Nano hyperspectral image. (b) Example RGB image. (c) Spatially averaged spectra extracted from the Nano image for the polygons digitized for each tank. (d) Spatially averaged pixel values extracted from the RGB image for the polygons digitized for each tank.

2.4. Relating Reflectance to Concentration via Optimal Band Ratio Analysis

Our analysis of the field spectra and image data sets acquired during this experiment focused on inferring the concentration of a visible tracer dye from the color of the water in the presence of varying levels of turbidity. To identify and exploit specific wavelength ranges that were highly sensitive to the amount of Rhodamine WT, we used an OBRA technique originally developed for retrieving water depth [12,14] but more recently applied to estimate dye concentrations from hyperspectral image data [10]. This method builds upon the ratio-based approach of Clark et al. [6] and involved calculating a log-transformed band ratio X , defined as

$$X = \ln \left[\frac{R(\lambda_1)}{R(\lambda_2)} \right], \quad (1)$$

for all possible combinations of numerator λ_1 and denominator λ_2 wavelengths, where $R(\lambda)$ denotes the reflectance or raw image digital numbers at wavelength λ . Given these X values, a separate regression of X against the corresponding in situ measurements of dye concentration C was performed for each band combination and the optimal band ratio was taken to be that pair of wavelengths that yielded the highest coefficient of determination R^2 . The regression equation associated with the optimal band ratio also provided a calibrated relationship for estimating dye concentration C from a spectrally based quantity X derived from field spectra or image data. In addition, we visualized the OBRA output as matrices that summarized spectral variations in the strength of the correlation between X and C . More specifically, we depicted the R^2 values for all band combinations in two-dimensional plots with axes for the numerator and denominator wavelengths and colors representing R^2 .

In this study, we performed OBRA of field spectra separately for each of the four turbidity ranges using all of the field spectra sets recorded while the turbidity was within a given range (Table 1). In each case, the response variable C for a given field spectra set was the mean (time-averaged over the 10-min duration of the measurement sequence) concentration, with the same mean value of C applied to all 40 of the individual field spectra within that set.

To assess the feasibility of inferring tracer concentrations from more readily available image data sets with a smaller number of broader bands, rather than continuous field spectra, we resampled the original 1 nm-resolution field spectra to the band passes of a representative multispectral sensor, the MicaSense RedEdge [24], and a high spatial resolution digital mapping camera, the Phase One iXM-100 [25] (Figure 3). These two sensors were selected because the USGS owns both of these instruments and the RedEdge and Phase One could thus be deployed during tracer studies planned for the Missouri River. Performing OBRA of the resampled field spectra provided an initial test of the potential to produce reliable maps of dye concentration from remotely sensed data acquired by these broader-band systems.

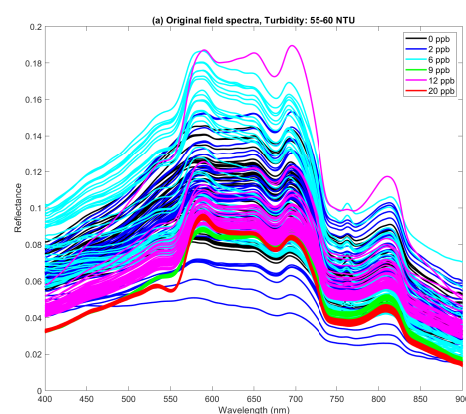


Figure 3. Cont.

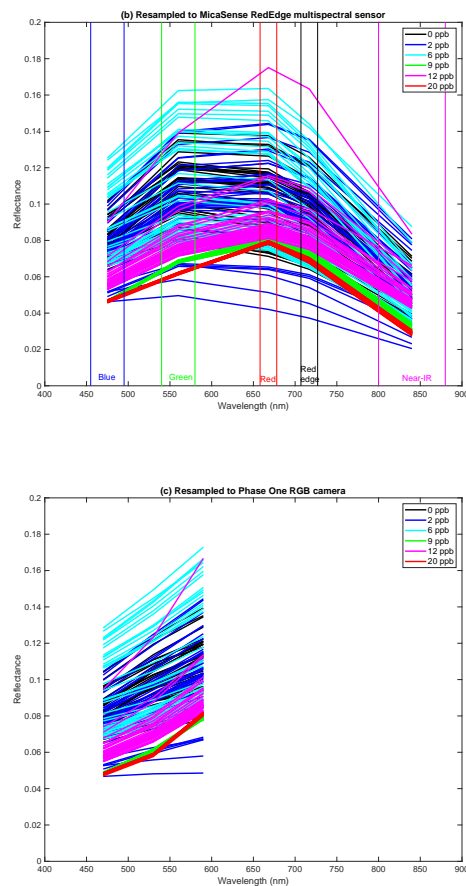


Figure 3. (a) Original field spectra for turbidity from 55–60 NTU and six different levels of dye concentration. (b) Spectra resampled to the band passes of the MicaSense RedEdge multispectral sensor. The band passes for the five bands of this instrument are indicated by vertical lines and labeled along the horizontal axis. (c) Spectra resampled to the band passes of the Phase One RGB camera.

3. Results

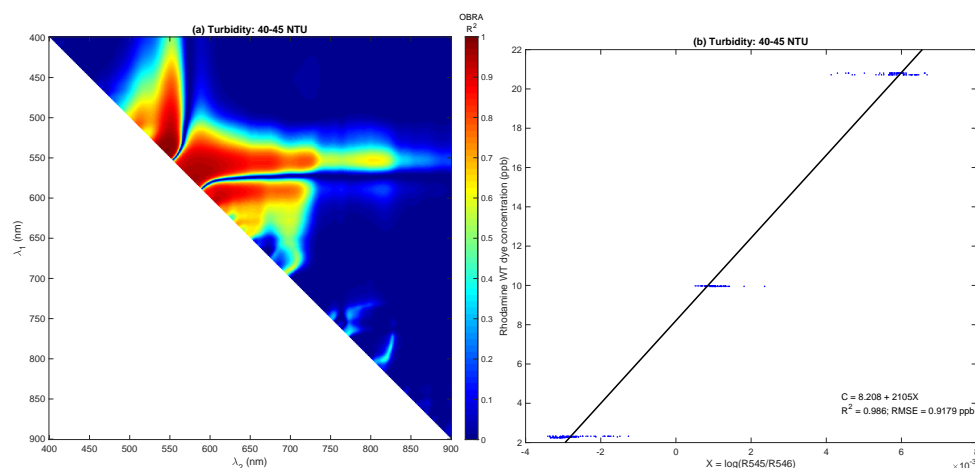
3.1. Optimal Band Ratio Analysis of Original and Resampled Field Spectra

As an initial test of the feasibility of retrieving tracer concentrations based on the reflectance characteristics of turbid river water, we performed OBRA of field spectra collected during an experiment in which both dye concentration and turbidity were manipulated as described above. The results of this analysis are summarized in Table 2 and illustrated graphically in Figure 4, where each row represents a different range of turbidity values. The OBRA matrices in the left column of Figure 4 graphically portray spectral variations in the strength of the relationship between the spectrally based quantity X , defined via Equation (1) for all possible combinations of numerator λ_1 and denominator λ_2 wavelengths, and in situ measurements of Rhodamine WT concentration C . The corresponding calibration scatter plots and regression output for the optimal band ratios (i.e., that which yielded the highest R^2) comprise the right column of Figure 4.

Table 2. Optimal band ratio analysis (OBRA) results for the original and resampled field spectra and hyperspectral and RGB images for each of the turbidity ranges observed during the experiment.

Data Type	Turbidity Range (NTU)	OBRA R^2	RMSE (ppb)	Numerator Wavelength (nm)	Denominator Wavelength (nm)	Slope	Intercept (ppb)
Original field spectra	40–45	0.986	0.918	545	546	2104.7	8.21
	45–50	0.983	0.744	543	545	1089.7	8.16
	50–55	0.974	0.882	575	586	−190.1	−0.40
	55–60	0.977	1.053	571	572	−933.3	−1.15
Field spectra resampled to MicaSense RedEdge multispectral	40–45	0.814	3.298	560	668	−70.7	7.61
	45–50	0.787	2.634	560	668	−67.0	5.84
	50–55	0.901	1.713	560	668	−75.5	2.68
	55–60	0.833	2.847	560	668	−56.2	4.73
Field spectra resampled to Phase One RGB bands	40–45	0.62	4.717	530	590	−101.4	−10.59
	45–50	0.607	3.581	530	590	−79.9	−7.19
	50–55	0.815	2.345	530	590	−80.4	−8.16
	55–60	0.842	2.771	530	590	−75.1	−5.49
Nano hyperspectral images acquired from sUAS	40–45	0.999	0.252	571.2	584.5	−212.6	−2.01
	45–50	0.996	0.429	555.6	593.4	−66.8	−2.19
	50–55	1	0.120	548.9	646.8	−106.1	−6.08
RGB images acquired from sUAS	40–45	0.949	1.721	650	550	98.2	−9.37
	45–50	0.952	1.458	650	550	81.4	−5.38
	50–55	0.889	2.016	650	550	71.2	−1.57

For all four turbidity ranges evaluated (40–45, 45–50, 50–55, and 55–60 NTU), OBRA yielded very strong linear relationships between X and C , with R^2 values ranging from 0.974 to 0.986 (Table 2). Moreover, the extensive bright red tones in the OBRA matrices indicated that broad ranges of wavelengths, not just the specific band combinations identified as optimal, also would yield X vs. C correlations nearly as strong (Figure 4). For example, using a green band around 555 nm as the numerator with any denominator band $555 > \lambda_2 > 700$ nm would provide an X vs. C $R^2 > 0.74$.

**Figure 4.** Cont.

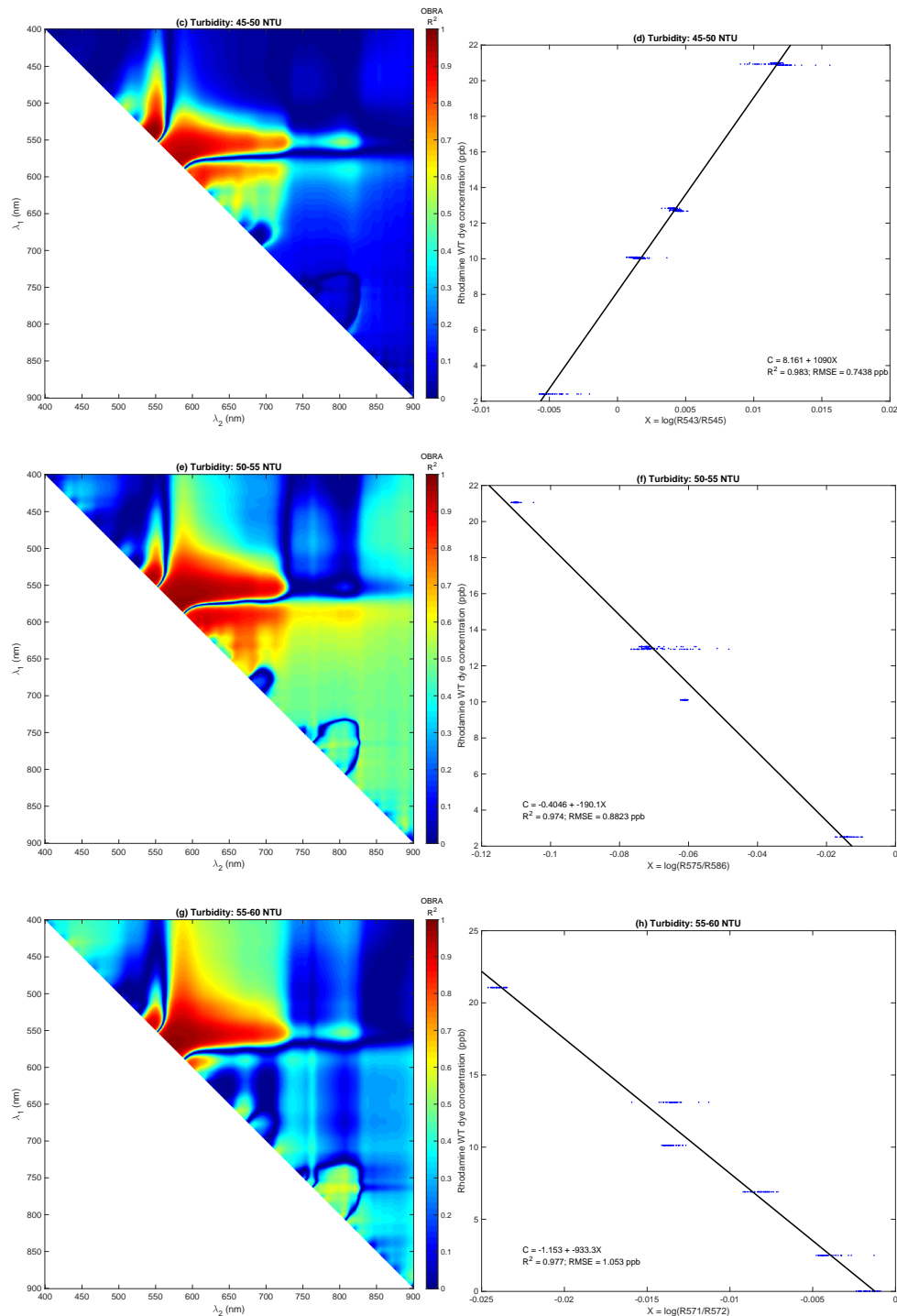


Figure 4. OBRA of field spectra stratified by turbidity range. The OBRA matrices in panels (a,c,e,g) illustrate spectral variations in the strength of the relationship between the spectrally based quantity X and dye concentration C . The calibration scatter plots and regression results for the corresponding optimal band ratios are shown in panels (b,d,f,h).

Although field spectra provided a useful starting point, ultimately we are interested in mapping dispersion patterns from various types of remotely sensed data. We, therefore, sought to assess the potential to estimate Rhodamine WT concentrations in the turbid waters of the Missouri River using a pair of multispectral sensors that are already in use by the USGS and representative of the kinds of instrumentation more readily available to other researchers and management agencies: the RedEdge

and Phase One imaging systems. Information on the sensor band passes of each instrument was used to resample the original field spectra to the five and three bands of the MicaSense and Phase One cameras, respectively (Figure 3). We then performed OBRA of the resampled spectra using the same six levels of concentration and four turbidity ranges as for the original field spectra. The results of this analysis are summarized in Table 2 and in figures that are analogous to Figure 4 and provided as Supplementary Materials associated with this paper (Figures S1 and S2).

For the RedEdge, which features three visible and two NIR bands, OBRA R^2 values varied from 0.787 for the 45–50 NTU turbidity range to 0.901 for the 50–55 NTU range, indicating strong relationships between the log-transformed band ratio X and Rhodamine WT concentration C across all turbidity levels considered. Moreover, the same green numerator and red denominator bands were identified as optimal for all four turbidity ranges. Whereas OBRA of the continuous field spectra suggested that a broad range of wavelengths would yield strong X vs. C correlations, the OBRA matrices for the resampled MicaSense RedEdge spectra illustrated in Figure S1 showed that $R(560)/R(668)$ (i.e., green/red) was the only band ratio consistently strongly related to concentration. The green/NIR (717 nm) ratio provided moderate X vs. C correlations and all other band combinations yielded only weak relationships.

Field spectra resampled to the RGB bands of the Phase One mapping camera yielded similar results but with weaker correlations between X and C . The OBRA R^2 was about 0.61 for the two lower turbidity ranges but rose to 0.815 and 0.842 for the 50–55 and 55–60 NTU ranges, respectively. The same band ratio was identified as optimal for all four turbidity ranges: $R(530)/R(590)$, essentially green/red given the wide bands of this RGB camera. The OBRA matrices in Figure S2 indicated that none of the other band combinations provided strong correlations.

3.2. Optimal Band Ratio Analysis of Hyperspectral and RGB Images

In addition to the measurements of reflectance made with the ground-based spectroradiometer, we also directly tested the ability to infer tracer concentrations from remotely sensed data by acquiring hyperspectral and RGB images from an sUAS during the experiment. Image data were available for the lower three turbidity ranges, but none of the images were acquired while the turbidity of the water in the two tanks was between 55 and 60 NTU. For the 40–45, 45–50, and 50–55 NTU turbidity ranges, we performed OBRA of the Nano and RGB images and the results of these analyses are summarized in Figures 5 and S3, respectively, as well as Table 2.

For the Nano images, the availability of many, narrow spectral bands allowed us to identify specific wavelength combinations that were very strongly related to Rhodamine WT dye concentrations, with OBRA R^2 values greater than 0.99 for all three turbidity ranges evaluated. The optimal band ratio varied among the different levels of turbidity (Table 2), but the OBRA matrices shown in the left column of Figure 5 included extensive dark red tones representing very strong correlations between X and C across a broad range of wavelengths; many other band combinations would yield relationships nearly as strong as that identified as optimal.

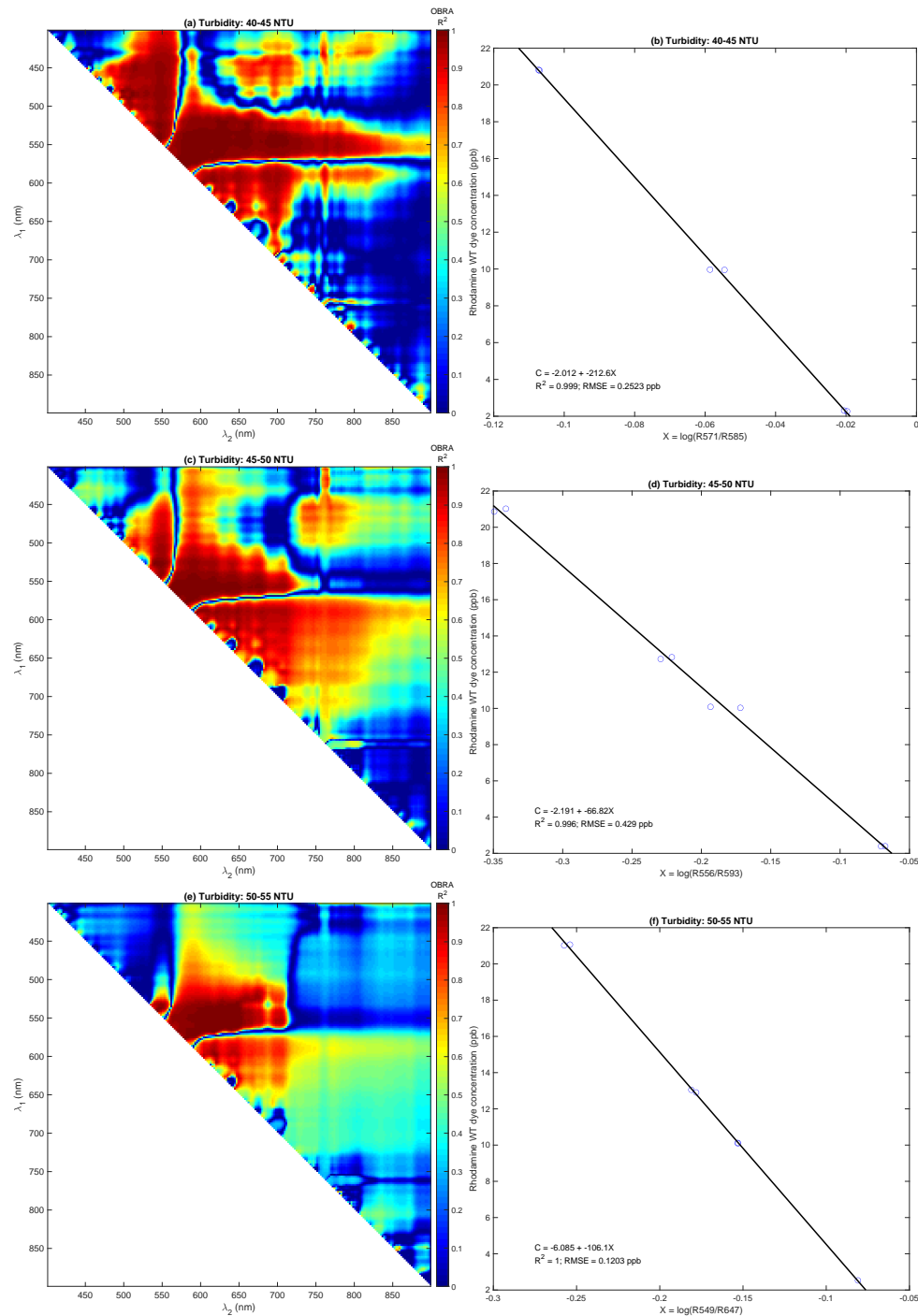


Figure 5. OBRA of small Unoccupied Aircraft System (sUAS)-based Nano hyperspectral images stratified by turbidity range.

More typical RGB images also were acquired from an sUAS during the experiment and OBRA of these relatively basic data lead to relationships between water color and dye concentration that were nearly as strong as those derived from the hyperspectral images. OBRA R^2 values for the sUAS-based RGB images were approximately 0.95 for the lower two turbidity ranges (40–45 and 45–50 NTU) and decreased only slightly to 0.889 for the highest of the three turbidity ranges for which image data were available (50–55 NTU, Table 2). RGB data can only be used to compute three unique band combinations, but the optimal band ratio identified via OBRA was red/green for all three levels of turbidity. The OBRA matrices shown in Figure S3 indicate that red/green yielded much stronger X vs. C correlations than the red/blue ratio, which in turn was far superior to the green/blue combination.

4. Discussion

4.1. Interpreting Relationships Between Reflectance and Concentration

Collecting field spectra during this experiment provided an efficient, focused means of examining relationships between reflectance and dye concentration at high spectral resolution and without the complicating factors associated with airborne image acquisition and processing. By acquiring hyperspectral and RGB images from an sUAS as part of the experiment, we also were able to directly evaluate the feasibility of retrieving dye concentrations from remotely sensed data, which is how this approach could be applied in practice to facilitate dispersion studies in turbid river channels. Analysis of these data sets, particularly the field spectra, not only demonstrated the potential to infer concentrations from observations of water color across a range of turbidity levels but also yielded novel insight regarding the nature of the correlation between the spectrally based quantity X and dye concentration C . In this section, we discuss these relationships for each type of data evaluated in this study: the original field spectra, field spectra resampled to the RedEdge and Phase One sensor bands, and the hyperspectral and RGB images acquired during the experiment.

For the original field spectra, the strength of the relationship between reflectance and concentration did not vary across the four turbidity ranges, but the sign of the correlation between X and C changed from positive for the 40–45 and 45–50 NTU turbidity ranges to negative for the two higher turbidity ranges, 50–55 and 55–60 NTU (Figure 4b,d,f,h; Table 2). For the lower two turbidity ranges, the optimal wavelengths used to define the band ratio X were centered around 545 nm and very close together, separated by only 1 or 2 nm. The adjacency of the two bands implied that the band ratio was essentially a derivative and could be interpreted as a spectral slope $dR(\lambda)/d\lambda$ (i.e., change in reflectance as a function of wavelength). Close inspection of the original field spectra, such as those illustrated in Figure 3a, indicated that $dR(\lambda)/d\lambda$ at 545 nm was most negative at high dye concentrations due to absorption by Rhodamine WT, became less negative for intermediate values of C , and was positive when the concentrations were lowest (i.e., 0 or 2 ppb) due to reduced absorption by the dye and a greater influence of the turbid water itself, the reflectance of which increased steadily throughout the green portion of the spectrum. At high concentrations, the decrease in reflectance with wavelength implied that $R(\lambda_1) > R(\lambda_2)$ for $\lambda_1 < \lambda_2$, leading to a ratio $R(\lambda_1)/R(\lambda_2) > 1$ and a positive value of the logarithm of the ratio (i.e., a positive value of X). For the lowest concentrations, the spectral slope was positive, implying that $R(\lambda_1) < R(\lambda_2)$, $R(\lambda_1)/R(\lambda_2) < 1$, and $X < 0$. The association of low concentrations with negative values of X and high concentrations with positive values of X thus resulted in a positive correlation between X and C .

For the two higher turbidity ranges, OBRA of the original field spectra identified longer wavelengths from 571–586 nm as optimal. These bands were located closer to the Rhodamine WT reflectance peak at approximately 590 nm and the spectral slope in this region thus was positive for all six concentration levels but less positive for lower concentrations. In this case, the positive slopes implied that $R(\lambda_1) < R(\lambda_2)$ for $\lambda_1 < \lambda_2$, leading to a band ratio value $R(\lambda_1)/R(\lambda_2) < 1$ and a negative value of the logarithm of the ratio (i.e., $X < 0$). The association of steeper positive spectral slopes with higher concentrations due to a more pronounced Rhodamine WT reflectance peak leads to larger negative values of X for greater values of C . For lower concentrations, the reflectance peak at 590 nm was not expressed as well and the gradual increase in reflectance with wavelength for the turbid water leads to more moderate spectral slopes and less negative values of X . Greater concentrations were thus associated with more negative values of X and lower concentrations with less negative values of X , leading to a negative correlation between X and C .

Only because we collected essentially continuous field spectra did these subtle details of the relationship between reflectance and concentration become evident. Although the X vs. C correlation changed from positive at lower turbidity ranges to negative at higher levels of turbidity, the algebraic sign of the correlation was of no practical significance. The key outcome of this analysis was that the relationship between the spectrally based quantity X and dye concentration C remained strong across

all four turbidity ranges. Our results thus implied that the inference of tracer concentrations from observations of spectral reflectance is not only feasible but potentially highly accurate, even in waters far more turbid than those examined in previous studies [10,11].

Using insight gained through analysis of the original field spectra as a guide, we also interpreted relationships between reflectance and Rhodamine WT concentration for resampled versions of the spectra intended to simulate the multispectral imaging systems that might be deployed to map dispersion patterns in practice. Whereas the original field spectra yielded both positive and negative correlations between X and C , resampling the spectra to the five MicaSense RedEdge bands lead to inverse relationships between the spectrally based quantity X and dye concentration for all four turbidity ranges (Table 2 and Figure S1). For the broader bands of this multispectral sensor, the absorption trough and reflectance peak of Rhodamine WT were not as distinct from one another, particularly since the band centered at 560 nm was located in an area of overlap between the absorption and reflectance spectra of the dye; this complicating factor also was identified by Clark et al. [6]. Examination of the resampled MicaSense RedEdge spectra in Figure 3b indicated that the spectral slope from the green to the red band was steeper for higher concentrations, leading to increasingly negative values of X and thus an inverse relationship between X and C . Similarly, when the original field spectra were resampled to the three bands of the Phase One camera, the absorption and reflectance features associated with Rhodamine WT were obscured to an even greater degree than for the RedEdge. Again, the spectral slope from the green to the red band was steeper for higher concentrations (Figure 3c), leading to inverse relationships between X and C (Table 2 and Figure S2).

The Nano hyperspectral images acquired from an sUAS during the experiment consisted of 272 bands and thus had a spectral resolution (2.2 nm sampling interval) nearly as high as the field spectra. As for the field spectra, this level of detail enabled us to identify band ratios very strongly correlated with dye concentration. The results summarized in Figure 5a,c,e indicated that many combinations of wavelengths would provide X vs. C R^2 values nearly as high as the optimum selected via OBRA, particularly for the two lower turbidity ranges evaluated. However, for the highest level of turbidity (50–55 NTU), wavelengths beyond approximately 700 nm were not useful as band ratio denominators, possibly due to a greater influence of more turbid water on NIR reflectance. For all three turbidity ranges, the optimal band ratio included at least one wavelength greater than 580 nm and thus near the Rhodamine WT reflectance peak around 590 nm. Because the spectral slope increased with dye concentration over the 540–590 nm range, $R(\lambda_1)$ was less than $R(\lambda_2)$, implying band ratio values $R(\lambda_1)/R(\lambda_2) < 1$ and $X < 0$, and leading to negative correlations between X and C . Whereas shorter wavelengths around 545 nm and thus closer to the Rhodamine WT absorption feature were selected for the field spectra for the lower two turbidity ranges, leading to positive X vs. C correlations, OBRA of the Nano images emphasized the reflectance peak associated with the dye and produced inverse relations between X and C across all three turbidity levels evaluated.

In addition to the Nano hyperspectral images, relatively basic RGB data from a sUAS also yielded strong relationships between water color and dye concentration. For the RGB images, OBRA R^2 values were as high as 0.95 and exceeded 0.88 for all three turbidity levels (Table 2), despite the much lower spectral resolution of these data, which dictated that only three unique band combinations were possible (Figure S3). Because the band sequence inherent to the RGB image files was not in order of increasing wavelength, the OBRA algorithm identified the red/green ratio as optimal. Given this definition of X with $R(\lambda_1) > R(\lambda_2)$, the relationships between X and C were direct for all three turbidity ranges. Had the ratio instead been defined as green/red, the strength of the correlations with C would have been the same but the X vs. C relations would have been inverse, as was the case for the hyperspectral images. In any case, the key outcome arising from this analysis was empirical evidence that reliable estimates of Rhodamine WT concentration could be derived from standard sUAS-based RGB images of turbid river channels.

4.2. Sensor Comparison and Implications for Image Data Acquisition to Support Tracer Experiments

The results of optimal band ratio analyses performed for the original and resampled field spectra and sUAS-based hyperspectral and RGB images are summarized and compared graphically in Figure 6 (Figure 6). For the essentially continuous field spectra with a 1 nm sampling interval, very strong relationships between X and C were observed for all four levels of turbidity. The Nano hyperspectral images produced even higher OBRA R^2 values than the field spectra for the 40–45, 45–50, and 50–55 NTU turbidity ranges. X vs. C correlations might have been stronger for the sUAS-based hyperspectral images than for the field spectra because Nano image pixel values were spatially averaged over the polygons digitized for each tank (Figure 2a), providing a more robust, less noisy sample of spectral reflectance than the field spectra, which were essentially instantaneous point measurements. Another factor contributing to the higher OBRA R^2 values for the Nano images might have been more favorable and consistent lighting conditions during the brief image acquisitions than during the longer duration field spectra measurement sets. In any case, our analysis of the sUAS-based hyperspectral images provided direct confirmation of the potential to map dye concentrations in turbid rivers via remote sensing.

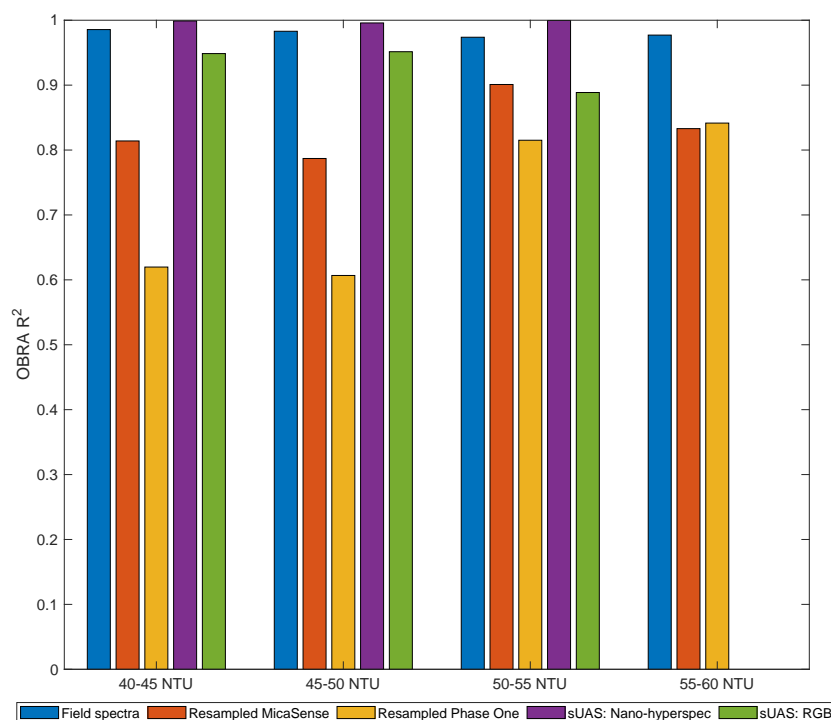


Figure 6. Summary of OBRA results for spectrally based dye concentration retrieval for varying levels of turbidity and types of sensor.

Resampling the original field spectra to simulate multispectral images further supported the notion of inferring dye concentrations from remotely sensed data. For example, field spectra resampled to the five bands of the MicaSense RedEdge instrument reduced the OBRA R^2 by as much as 0.2 for the 45–50 NTU turbidity range, but R^2 values of 0.787 or better indicated that the reduced spectral resolution of the RedEdge did not seriously compromise the ability to estimate dye concentration from observations of water color. Similarly, although resampling the field spectra to the RGB bands of the Phase One camera weakened the X vs. C relation to a greater degree, with a reduction in OBRA R^2 of up to 0.38, our analyses suggested that moderately strong correlations could be derived from this type of basic, readily available image data. Moreover, for the resampled Phase One spectra the OBRA R^2 values were approximately 0.2 higher for the two higher turbidity ranges (50–55 and 55–60 NTU)

than the two lower turbidity ranges (40–45 and 45–50 NTU), suggesting that this type of sensor might provide more accurate dye concentration estimates in more turbid water.

The sUAS-based RGB images acquired during the experiment more directly demonstrated the feasibility of mapping the dispersion of dye in turbid river channels. OBRA R^2 values ranged from 0.889 at the highest level of turbidity (50–55 NTU) for which image data were available to 0.95 for the lower two turbidity levels (40–45 and 45–50 NTU). Similar to the superior performance of the Nano compared to the field spectra, the sUAS-based RGB images acquired during the experiment yielded higher OBRA R^2 values than field spectra resampled to the RGB bands of the Phase One camera. As for the Nano, spatial averaging of the sUAS-based RGB image pixel values within the tank polygons would have improved the signal-to-noise characteristics of the images recorded by the camera aboard the sUAS relative to the resampled field spectra. Again, better lighting during image acquisition also could have contributed to stronger X vs. C correlations for the sUAS-based images. Another factor that might in part explain the disparate OBRA R^2 values could be differences between the sensor response functions of the Phase One system and the built-in DJI camera on the sUAS, essentially how the two sensors weighted various visible wavelengths to obtain pixel values in their respective, nominal red, green, and blue bands.

Although the relationships between reflectance and concentration were not quite as strong for the sUAS-based RGB images as for the hyperspectral images, the results of this study imply that accurate estimates of Rhodamine WT concentration could be derived from standard RGB data acquired by common, inexpensive instruments. If highly precise concentration retrieval is essential to the objectives of a particular investigation, hyperspectral data might be the preferred option but for most practical applications the results of this experiment suggest that more widely available RGB image data might be sufficient. In addition to their greater accessibility, lower cost, and simpler processing workflows, RGB systems typically also provide higher spatial resolution (i.e., smaller pixel sizes for a given flying height) than hyperspectral sensors, which could be an important consideration for mapping complex dispersion patterns in eddies and other small-scale features of the flow field.

4.3. Limitations and Applicability

This proof-of-concept investigation yielded some encouraging initial results but was limited in at least one very important respect. The band ratio-based approach we employed is fundamentally an empirical technique and thus not truly general. The output from OBRA is essentially a calibration relation that is specific to the data set provided as input to the algorithm and not directly transferable to other sites. Although OBRA provides a useful, practical framework suitable for application on a case-by-case basis, any project that adopts this method will need to obtain site-specific field measurements of dye concentration for calibrating a relationship between X and C . Greater flexibility could be achieved by establishing the biophysical basis for a particular band ratio that exploits the reflectance and absorption features of a visible tracer dye to provide a strong, robust, and highly portable linkage between some spectrally based quantity and dye concentration. In this study, the selection of different optimal band ratios for different sensors and turbidity levels (Table 2) based on strong statistical correlations between X and C for the various definitions of X implied that the relations were data-driven and did not provide evidence of causation, only correlation.

Working toward a more general, physics-based approach to remote sensing of tracer dye concentrations thus emerged as an important topic for further investigation. For the time being, however, the OBRA framework provides an efficient empirical means of identifying an appropriate band ratio for a particular data set and establishing a useful calibration relation for a given project. A greater understanding of the combined, interacting effects of background water characteristics and the optical properties of the dye is needed to establish a more universal, reliable relationship between reflectance and concentration suitable for routine application to remotely sensed data from a range of river environments. Demonstrating algorithm consistency across data sets from different streams and sensors will be an important step toward achieving this important objective.

4.4. Future Research Directions

Although this study provided strong evidence that reliable estimates of dye concentration could be derived from observations of water color even in the presence of greater turbidity, this initial test was performed under controlled experimental conditions. Our research was motivated by the longer-term objective of mapping dispersion patterns along the Missouri River to support ongoing investigations of the movement of endangered pallid sturgeon larvae. A related goal is to assess the performance of habitat improvement projects constructed on several reaches of the Missouri River. Based on the results of this experiment, we plan to move forward with a coordinated field campaign that will involve releasing a pulse of Rhodamine WT into the channel and monitoring its spread via both in situ sondes deployed at several fixed locations to record the passage of the dye over time and remotely sensed data intended to capture spatial patterns. To document the small-scale dynamics of the dispersion process at one of the habitat improvement sites, we are considering deploying an sUAS in a hovering mode to obtain an image time series. In addition, to capture the movement of the dye plume at several points in time, we intend to use a faster manned aircraft with greater range to acquire repeat coverage over a longer (5–10 km) reach of the river. This approach could yield novel insight regarding the early life stages of the sturgeon species of concern and also provide a unique opportunity to validate numerical models of the dispersion process. In addition, the study planned for the Missouri River will provide a direct evaluation of the feasibility of measuring tracer concentrations via remote sensing under field conditions in a large, turbid channel.

5. Conclusions

To assess the feasibility of estimating tracer concentrations from remotely sensed data in more turbid rivers than those examined previously, we performed an experiment that involved manipulating dye concentration and turbidity while acquiring ground-based field spectra and hyperspectral and RGB images from an sUAS. Our results support the following conclusions:

1. Reliable estimates of Rhodamine WT dye concentration can be inferred from observations of reflectance (i.e., water color), even in the presence of higher levels of turbidity (40–60 NTU) than considered in previous studies conducted on clear-flowing streams.
2. Applying an empirical OBRA algorithm to essentially continuous ground-based field spectra and spectra resampled to the bands of multispectral and RGB images yielded strong correlations between a spectrally based quantity (i.e., a band ratio) and dye concentration across four different turbidity ranges (40–45, 45–50, 50–55, and 55–60 NTU).
3. Although OBRA identified a specific, optimal pair of wavelengths for each data set, analysis of the original field spectra indicated that a broad range of wavelengths would provide reflectance vs. concentration relations nearly as strong, implying that a large number of narrow spectral bands is not necessary for accurate concentration retrieval.
4. OBRA of field spectra resampled to a five-band multispectral imaging system and an RGB camera provided further evidence that broader-band sensors are sufficient for mapping dye concentrations in turbid waters.
5. Both hyperspectral and RGB images acquired from an sUAS during the experiment yielded strong relationships between spectrally based quantities and in situ measurements of dye concentration, implying that remote sensing is a viable approach to mapping dispersion patterns in turbid river channels.

Supplementary Materials: The following are available online at <http://www.mdpi.com/2072-4292/12/1/57/s1>, Figure S1: Optimal Band Ratio Analysis (OBRA) of field spectra resampled to the band passes of the MicaSense RedEdge multispectral sensor and stratified by turbidity range. Figure S2: Optimal Band Ratio Analysis (OBRA) of field spectra resampled to the band passes of the Phase One RGB camera and stratified by turbidity range. Figure S3: Optimal Band Ratio Analysis (OBRA) of sUAS-based RGB images stratified by turbidity range.

Author Contributions: Conceptualization, C.J.L., S.O.E., and E.A.B.; methodology, C.J.L., P.V.M., E.A.B., and S.O.E.; software, C.J.L.; validation, C.J.L., P.V.M., S.O.E., and E.A.B.; formal analysis, C.J.L., P.V.M., S.O.E., and

E.A.B.; investigation, C.J.L., S.O.E., and E.A.B.; resources, C.J.L., P.V.M., S.O.E., and E.A.B.; data curation, C.J.L.; writing—original draft preparation, C.J.L., P.V.M., and E.A.B.; writing—review and editing, P.V.M., S.O.E., and E.A.B.; visualization, C.J.L.; supervision, S.O.E.; project administration, S.O.E.; funding acquisition, S.O.E. All authors have read and agreed to the published version of the manuscript.

Funding: Funding for this study was provided by the U.S. Army Corps of Engineers Missouri River Recovery Integrated Science Program and the U.S. Geological Survey Ecosystems and Water Mission Areas.

Acknowledgments: Several technicians at the USGS Columbia Environmental Research Center contributed to this work, most notably but not limited to Maura Roberts, Tyrell Helmuth, and Brian Anderson. Any use of trade, firm, or product names is for descriptive purposes only and does not imply endorsement by the U.S. Government.

Conflicts of Interest: The authors declare no conflict of interest.

References

- Seo, I.W.; Choi, H.J.; Kim, Y.D.; Han, E.J. Analysis of Two-Dimensional Mixing in Natural Streams Based on Transient Tracer Tests. *J. Hydraul. Eng.* **2016**, *142*, 4016020. [[CrossRef](#)]
- Nelson, J.; McDonald, R.; Legleiter, C.; Kinzel, P.; Terrell-Ramos, T.; Higashi, Y.; Seo, I.W.; Baek, D.; Lee, D.H.; Ryu, Y. New methods for predicting and measuring dispersion in rivers. *E3S Web Conf.* **2018**, *40*, 05052. [[CrossRef](#)]
- Lewitus, A.J.; Horner, R.A.; Caron, D.A.; Garcia-Mendoza, E.; Hickey, B.M.; Hunter, M.; Huppert, D.D.; Kudela, R.M.; Langlois, G.W.; Largier, J.L.; et al. Harmful algal blooms along the North American west coast region: History, trends, causes, and impacts. *Harm. Algae* **2012**, *19*, 133–159. [[CrossRef](#)]
- Erwin, S.O.; Bulliner, E.A.; Fischelich, J.C.; Jacobson, R.B.; Braaten, P.J.; DeLonay, A.J. Evaluating flow management as a strategy to recover an endangered sturgeon species in the Upper Missouri River, USA. *River Res. Appl.* **2018**, *34*, 1254–1266. [[CrossRef](#)]
- Runkel, R.L. On the use of rhodamine WT for the characterization of stream hydrodynamics and transient storage. *Water Resour. Res.* **2015**, *51*, 6125–6142. [[CrossRef](#)]
- Clark, D.B.; Lenain, L.; Feddersen, F.; Boss, E.; Guza, R.T. Aerial Imaging of Fluorescent Dye in the Near Shore. *J. Atmos. Ocean. Technol.* **2014**, *31*, 1410–1421. [[CrossRef](#)]
- Feddersen, F.; Olabarrieta, M.; Guza, R.T.; Winters, D.; Raubenheimer, B.; Elgar, S. Observations and modeling of a tidal inlet dye tracer plume. *J. Geophys. Res. Oceans* **2016**, *121*, 7819–7844. [[CrossRef](#)]
- Viriot, M.L.; Andre, J.C. Fluorescent dyes: A search for new tracers for hydrology. *Analysis* **1989**, *17*, 97–111.
- Powers, C.; Hanlon, R.; Schmale, D. Tracking of a Fluorescent Dye in a Freshwater Lake with an Unmanned Surface Vehicle and an Unmanned Aircraft System. *Remote Sens.* **2018**, *10*, 81. [[CrossRef](#)]
- Legleiter, C.J.; McDonald, R.R.; Nelson, J.M.; Kinzel, P.J.; Perroy, R.L.; Baek, D.; Seo, I.W. Remote sensing of tracer dye concentrations to support dispersion studies in river channels. *J. Ecohydraul.* **2019**. [[CrossRef](#)]
- Baek, D.; Seo, I.W.; Kim, J.S.; Nelson, J.M. UAV-based measurements of spatio-temporal concentration distributions of fluorescent tracers in open channel flows. *Adv. Water Resour.* **2019**, *127*, 76–88. [[CrossRef](#)]
- Legleiter, C.J.; Roberts, D.A.; Lawrence, R.L. Spectrally based remote sensing of river bathymetry. *Earth Surf. Process. Landf.* **2009**, *34*, 1039–1059. [[CrossRef](#)]
- Legleiter, C.J.; Harrison, L.R. Remote Sensing of River Bathymetry: Evaluating a Range of Sensors, Platforms, and Algorithms on the Upper Sacramento River, California, USA. *Water Resour. Res.* **2019**, *55*, 2142–2169. [[CrossRef](#)]
- Legleiter, C.; Fosness, R. Defining the Limits of Spectrally Based Bathymetric Mapping on a Large River. *Remote Sens.* **2019**, *11*, 665. [[CrossRef](#)]
- Jacobson, R.B.; Annis, M.L.; Colvin, M.E.; James, D.A.; Welker, T.L.; Parsley, M.J. *Missouri River Scaphirhynchus albus (Pallid Sturgeon) Effects Analysis—Integrative Report 2016*; Scientific Investigation Report 2016-5064; US Geological: Reston, VA, USA, 2016.
- Legleiter, C.J.; Manley, P.; Erwin, S.O.; Bulliner, E.A. Field spectra, UAS-based hyperspectral and RGB images, and in situ measurements of turbidity and Rhodamine WT dye concentration from an experiment conducted at the USGS Columbia Environmental Research Center, Columbia, MO, on April 2, 2019. *U.S. Geol. Surv. Data Release* **2019**. [[CrossRef](#)]
- ASD HandHeld 2 Pro: VNIR Hand-Held Spectroradiometer. Available online: <https://www.malvernpanalytical.com/en/support/product-support/asd-range/fieldspec-range/handheld-2-pro-vnir-hand-held-spectroradiometer/index.html> (accessed on 29 August 2019).

18. Spectralon Diffuse Reflectance Standards—Labsphere. Available online: <https://www.labsphere.com/labsphere-products-solutions/materials-coatings-2/targets-standards/diffuse-reflectance-standards/diffuse-reflectance-standards/> (accessed on 29 August 2019).
19. Hyperspectral Sensors. Available online: <http://www.headwallphotonics.com/hyperspectral-sensors> (accessed on 29 August 2019).
20. DJI Matrice 600 Pro. Available online: <https://www.dji.com/matrice600-pro> (accessed on 29 August 2019).
21. DJI Ronin-MX — Capture Above and Beyond. Available online: <https://www.dji.com/ronin-mx> (accessed on 29 August 2019).
22. ENVI— The Leading Geospatial Analytics Software—Harris Geospatial. Available online: <https://www.harrisgeospatial.com/Software-Technology/ENVI> (accessed on 29 August 2019).
23. DJI Mavic Pro & Mavic Pro Platinum—Every Creative Moment. Available online: <https://www.dji.com/mavic> (accessed on 29 August 2019).
24. RedEdge-MX—MicaSense. Available online: <https://www.micasense.com/rededge-mx> (accessed on 29 August 2019).
25. Phase One Industrial iXM-100/iXM-50. Available online: https://industrial.phaseone.com/\iXM_Camera_Series.aspx (accessed on 29 August 2019).



© 2019 by the authors. Licensee MDPI, Basel, Switzerland. This article is an open access article distributed under the terms and conditions of the Creative Commons Attribution (CC BY) license (<http://creativecommons.org/licenses/by/4.0/>).